Energy Storage and Conversion 2026, 4(3), 4726.
doi: https://doi.org/10.59400/esc4726

Article

Comparative analysis of steady-state and dynamic models for grid-connected photovoltaic farm performance monitoring: A case study of Huawei SUN2000-60KTL-M0 inverter

Dias Prihatmoko[1,2,*], Rustam Asnawi[3], Moh. Khairudin[3], Nor Azlan Othman[4]

[1] Doctoral Program of Engineering Science, Faculty of Engineering, Universitas Negeri Yogyakarta, Yogyakarta 55281, Indonesia
[2] Department of Electrical Engineering, Universitas Islam Nahdlatul Ulama Jepara, Jepara 59424, Indonesia
[3] Department of Electrical Engineering, Faculty of Engineering, Universitas Negeri Yogyakarta, Yogyakarta 55281, Indonesia; rustam@uny.ac.id (RA); moh_khairudin@uny.ac.id (MK)
[4] Faculty of Mechanical Engineering, Universiti Teknologi MARA, Shah Alam 40450, Malaysia; azlan253@uitm.edu.my
* **Corresponding author:** Dias Prihatmoko, diasprihatmoko@unisnu.ac.id

CITATION

Prihatmoko D, Asnawi R, Khairudin M, et al. Comparative analysis of steady-state and dynamic models for grid-connected photovoltaic farm performance monitoring: A case study of Huawei SUN2000-60KTL-M0 inverter. Energy Storage and Conversion. 2026; 4(3): 4726. https://doi.org/10.59400/esc4726

ARTICLE INFO

Received: 27 July 2026
Revised: 16 August 2026
Accepted: 21 August 2026
Available online: 25 August 2026

Abstract: This study evaluates the solar-to-electrical energy conversion performance of a 63.24 kWp grid-connected photovoltaic (PV) farm equipped with a Huawei SUN2000-60KTL-M0 (60 kW) inverter by comparing a steady-state diagnostic model against a dynamic observability assessment. A single-instant snapshot of 12 PV strings on 26 June 2026 identified three non-producing strings (PV6, PV7, PV8), reducing string availability to 75.0% and causing an instantaneous DC power shortfall of approximately 6.0 kW (23.6% of currently achievable capacity). Inverter DC-to-AC conversion efficiency was 98.72% and the observed daily-equivalent capacity factor was 15.48%, both computed directly from measured values. Performance Ratio is reported as not evaluable due to the absence of temporally overlapping plane-of-array irradiance data. The dynamic assessment evaluates day-to-day energy temporal variability and historical hourly weather variability from measured June 2026 and 2020–2025 records (mean absolute daily ramp 12.66%, daily energy CV 19.45%), while sub-minute electrical transient characteristics remain not evaluable owing to the lack of sub-minute electrical logging. A Model Observability Score (MOS) and Data Resolution Adequacy Index (DRAI) are computed from an a priori parameter registry. The steady-state model achieves an MOS of 87.5% (7 of 8 applicable parameters), while the dynamic model achieves 25.0% (4 of 16), with the gap concentrated in the electrical-transient domain and attributable to instrumentation limitations. A phased instrumentation roadmap is proposed. The findings provide a transparent, auditable template for determining appropriate monitoring depth in tropical grid-connected PV operations and maintenance practice.

Keywords: photovoltaic monitoring; steady-state model; dynamic model; performance ratio; grid-connected PV

1. Introduction

The rapid global deployment of photovoltaic (PV) systems has intensified the need for robust performance-monitoring frameworks that can identify anomalies, quantify performance losses, and support preventive maintenance [1, 2]. Grid-connected PV systems are intrinsically influenced by irradiance, temperature, shading, component condition, and inverter behavior [3]. Two analytical layers are particularly relevant to this study: steady-state analysis, which characterizes an operating point or aggregated performance state, and dynamic analysis, which requires time-resolved measurements to characterize temporal or transient behavior [1].

Photovoltaic performance assessment goes beyond simple system supervision and requires performance indicators that are consistent with the available measurement channels. Performance Ratio (PR), energy yield, inverter conversion efficiency, and related monitoring quantities are widely used, but their validity depends on the completeness and temporal alignment of the underlying measurements [4, 5]. In particular, PR requires an irradiance-based reference yield that overlaps the electrical-output period; transient-response characterization requires sufficiently time-resolved electrical measurements.

Dynamic PV and inverter assessment therefore requires a sampling interval appropriate to the phenomenon being studied, together with synchronized electrical and, where relevant, irradiance measurements [6–8]. By contrast, plant monitoring at slower time scales remains useful for operating-point assessment, energy accounting, and anomaly screening when the interpretation is kept within the limits of those data [1,4]. The present site does not contain the high-frequency electrical channels required for true transient identification; that absence is treated as an observability limitation rather than filled with assumed values. A systematic, auditable framework for deciding which monitoring layer is actually supported by a site's data remains especially useful for operational PV studies.

This paper revisits the JST PV Farm case study, a 63.24 kWp installation with a Huawei SUN2000-60KTL-M0 inverter, with that observability-first principle as its organizing idea. On 26 June 2026, actual snapshot monitoring data showed three simultaneously non-producing PV strings. Rather than filling data gaps with assumed peak-sun-hour values, an assumed inverter time constant, or an invented thermal reading, this revised analysis reports each metric strictly according to what the available data can support, and treats the resulting gap between the steady-state and dynamic models as a quantifiable instrumentation deficit rather than a narrative device. The specific contributions of this work are: (1) a string-level, measurement-only anomaly screening that avoids attributing definitive root causes to a single V–I snapshot; (2) an explicit resolution-versus-requirement assessment establishing, transparently, why sub-minute dynamic characterization is not currently supported at this site; (3) a Model Observability Score (MOS) and Data Resolution Adequacy Index (DRAI) that quantify the steady-state/dynamic observability gap without any arbitrary combined weighting between the two paradigms; and (4) a phased instrumentation roadmap that ties each proposed sensor investment to the specific observability gap it would close.

2. Literature review

Steady-state PV modeling is commonly grounded in the electrical behavior of the PV array and, when physics-based prediction is required, the single-diode representation [9]. For monitored grid-connected systems, PR is a widely used performance indicator, but its value is sensitive to the irradiance measurement used to construct the reference yield [4, 5]. Long-term degradation analysis likewise requires careful data qualification, filtering, normalization, and trend estimation; different methodologies can produce materially different degradation-rate estimates [10,11]. At the DC side, monitored string-current and voltage signatures are useful for screening underperforming strings, while the literature distinguishes screening or detection from definitive physical root-cause confirmation [12–14].

The classical PV-array modeling work of Villalva et al. provides a well-established basis for representing nonlinear photovoltaic electrical behavior [9]. Dynamic MPPT performance, however, is normally evaluated with deliberately time-varying irradiance profiles and time-resolved measurements or experiments. Phinikarides et al. compared MPPT algorithms under the EN50530 dynamic test procedure [10], while Ahmed and Salam evaluated tracking performance under changing irradiance using standardized dynamic profiles [15]. Belkaid et al. specifically studied MPPT behavior under fast-varying solar radiation [16]. Separately, Lappalainen and Valkealahti characterized irradiance transitions caused by moving clouds from measured irradiance data [17]. More recent data-driven experiments have shown that inverter dynamic behavior can depend on irradiance level and operating mode, reinforcing the need for measured time-series data when identifying inverter dynamics [14].

Taken together, these studies support two methodological points used in the present revision. First, dynamic conclusions should be based on time-resolved measurements whose sampling rate is appropriate to the transient phenomenon [7, 13, 16]. Second, string-level monitoring can still provide useful diagnostic screening from electrical measurements alone, provided the interpretation is limited to measured-condition signatures rather than an unverified root cause [9,10]. The contribution of this paper is therefore not a new transient inverter equation, but an observability-first comparison that makes the boundary between evaluated and non-evaluated quantities explicit and auditable.

Despite these individual contributions, no prior study has systematically compared steady-state and dynamic modeling suitability using an explicit, auditable observability metric rather than a narrative judgment within a single operational tropical case study. This paper addresses that gap.

3. Methodology

3.1. System description and data acquisition

The JST PV Farm consists of a single Huawei SUN2000-60KTL-M0 inverter rated at 60 kW AC, connected to 12 PV strings, each comprising 17 series-connected 310 Wp monocrystalline modules, yielding a nominal DC array capacity of 63.24 kWp. String-level monitoring data (voltage, current) were acquired from the Huawei FusionSolar monitoring platform at timestamp 2026-06-26 08:16:27 WIB, supplemented by 26 daily energy records for June 2026 (23 valid full-day records, 2 No-Data days, 1 partial day) and annual energy totals for 2022–2026 (2026 partial). Grid-connection parameters (power factor, frequency) were obtained from inverter Modbus registers. No independent irradiance sensor (pyranometer), ambient- or inverter-temperature sensor, or high-frequency (sub-minute) data logger was available at the site at the time of this study; this absence is treated as a primary methodological constraint throughout, rather than filled by an external or assumed value.

3.2. Steady-state diagnostic framework

String-level operating points were computed directly from measured voltage–current (V–I) pairs according to

$$P = V \times I \tag{1}$$

with no string-level power value assumed or interpolated. Each string was assigned a purely descriptive measured-condition label producing, zero current/high voltage or zero current/low based solely on its own snapshot voltage and current. These labels intentionally stop short of a confirmed physical root-cause diagnosis (e.g., blown fuse, bypass-diode activation, or module damage), which a single V–I snapshot cannot, by itself, establish without complementary evidence such as I–V curve tracing or thermal imaging.

System-level key performance indicators (KPIs) were derived as follows:

Inverter Efficiency:

$$\eta_{\text{inv}} = \frac{P_{\text{ac}}}{P_{\text{dc}}} \times 100\% \tag{2}$$

Capacity Factor:

$$\text{CF} = \frac{E_{\text{full-day-mean}}}{P_{\text{array}} \times 24} \times 100\% \tag{3}$$

where is the mean measured daily energy across full-day, non-interrupted records in the June 2026 log. No-Data and partial-day records are excluded from this mean and are not interpolated.

Performance Ratio:

$$\text{PR} = \frac{E_{\text{ac}}}{G_{\text{POA}} \times A \times \eta_{\text{STC}}} \tag{4}$$

requires a plane-of-array irradiance record that temporally overlaps the PV output period. Because no such record exists at this site the only available irradiance archive predates the June 2026 monitoring window and does not overlap it PR is reported as NOT EVALUATED rather than approximated from an assumed or externally sourced peak-sun-hour (PSH) value.

Financial-impact figures, where reported, are computed from the measured snapshot power shortfall using the PLN industrial tariff of Rp 1,500/kWh [1], and are explicitly labeled as illustrative, single-scenario estimates rather than validated annual figures (Section 4.3).

3.3. Dynamic observability assessment framework

The dynamic assessment in this study is deliberately not a single pass/fail verdict. Three distinct classes of dynamic phenomenon are distinguished, each with its own data-resolution requirement: (i) day-to-day energy temporal variability, which requires only daily-resolution logging and is therefore genuinely evaluable from the existing June 2026 daily energy log; (ii) historical environmental variability, which requires hourly-resolution weather logging and is genuinely evaluable from the existing 2020–2025 archive (though not temporally paired with the June 2026

PV output); and (iii) true electrical transient behavior power ramp-rate, inverter response time, and grid transient/rate-of-change of frequency (RoCoF) which requires sub-minute-to-sub-second electrical logging that this site does not have. For each of these five specific phenomena, a declared required sampling interval, Δt_required, is specified a priori, with literature or standards support where applicable and compared against the site's actual sampling interval, Δt_actual, measured strictly from each dataset's own timestamps. Because the electrical channel has no timestamp at all, Δt_actual is undefined not merely large for the three electrical-transient phenomena; this is reported as NOT_EVALUATED, distinct from a defined-but-inadequate resolution, since no timestamp exists against which to compute one. No inverter time constant, MPPT reaction time, or cloud-shadow irradiance profile is assumed anywhere in this framework.

3.4. Comparative observability framework: MOS and DRAI

To situate the steady-state and dynamic results against one another without introducing an arbitrary combined score, two transparent, count-based constructs are employed. Both are computed from a fixed, a priori parameter registry rather than from a denominator chosen after inspecting the results.

Model Observability Score (MOS) for model m is defined as:

$$\mathrm{MOS}_m = \frac{N_{\text{evaluated},m}}{N_{\text{applicable},m}} \times 100\% \tag{5}$$

This is a pure count of how many parameters applicable to model $m$were actually evaluated (i.e., status EVALUATED, not NOT_EVALUATED) from the model's own output, with no subjective weighting applied. Parameters marked NOT_APPLICABLE to a given model are excluded from that model's denominator entirely, and a POTENTIAL status is never automatically counted as evaluated. The registry declares each parameter's applicability to the steady-state model and to the dynamic model independently and before the results are computed, so that $\mathrm{MOS}_{\mathrm{SS}}$ and $\mathrm{MOS}_{\mathrm{Dynamic}}$ are read from disjoint columns of the same table and can be audited row-by-row.

Data Resolution Adequacy Index (DRAI) for phenomenon is defined as:

$$\mathrm{DRAI}_j = \min\left(1,\ \frac{\Delta t_{\text{required},j}}{\Delta t_{\text{actual},j}}\right) \tag{6}$$

This index compares each phenomenon's actual sampling interval against its declared requirement. DRAI is left undefined not set to zero when cannot be computed.

Neither construct is combined into a single ranked score between the steady-state and dynamic models. The two remain reported as separate, complementary diagnostics (Section 4.7).

4. Results and discussion

4.1. String-level measured-condition analysis

Table 1 summarizes the string operating parameters measured on 26 June 2026, 08:16 WIB. Point: three of the twelve strings PV6, PV7, and PV8 registered zero current, reducing snapshot string availability to 75.0% (9 of 12 strings). Evidence: PV6 registered 625.8 V at zero current, while PV7 and PV8 registered a markedly lower voltage (149.3 V), also at zero current; together, the three strings account for an instantaneous DC shortfall of approximately 6,000 W relative to the array's currently achievable capacity at this snapshot. The nine producing strings operated between 585.7 and 625.8 V (mean 597.8 V), with currents between 3.11 and 6.66 A, indicating substantial inter-string current non-uniformity at the observed operating point, which cannot be attributed to irradiance non-uniformity in the absence of a temporally overlapping irradiance measurement. Reasoning: consistent with the descriptive-labeling principle in Section 3.2, PV6's zero-current/high-voltage signature and PV7/PV8's zero-current/low-voltage signature are reported as two distinct measured conditions not as confirmed physical diagnoses. PV monitoring literature supports string-current and voltage-based screening, while also requiring additional evidence for robust fault localization and classification [12–14]. Conclusion: PV6 and PV7/PV8 are therefore treated as separate inspection priorities rather than a single confirmed fault class. The aggregated calculated string power was 25.493 kW, closely matching the inverter-reported DC input of 25.361 kW (0.521% difference), while the AC output of 25.036 kW yielded a calculated inverter efficiency of 98.719%. The value is consistent with the high conversion efficiency stated in the manufacturer's SUN2000-60KTL-M0 technical data [18–21].

Table 1. PV string operating parameters and measured condition (2026-06-26 08:16 WIB).

String ID	Voltage (V)	Current (A)	Power (W)
PV1	598.0	4.20	2,511.6
PV2	598.0	3.92	2,344.2
PV3	607.9	3.68	2,237.1
PV4	607.9	3.51	2,133.7
PV5	625.8	3.11	1,946.2
PV6	625.8	0.00	0.0
PV7	149.3	0.00	0.0
PV8	149.3	0.00	0.0
PV9	585.7	5.44	3,186.2
PV10	585.7	5.91	3,461.5
PV11	585.7	6.44	3,771.9
PV12	585.7	6.66	3,900.6

4.2. Steady-state key performance indicators

Point: the steady-state KPIs computed directly from measured data (**Table 2**) show high instantaneous inverter conversion efficiency but reduced string availability. Evidence: monthly cumulative energy for June 2026 was 5,429 kWh, and the mean full-day energy across valid records was 234.96 kWh/day, giving an observed daily-equivalent Capacity Factor of 15.48%. This CF is reported as a site-specific observed indicator rather than compared with an unsupported universal tropical benchmark. Inverter efficiency was 98.72%, close to the manufacturer's stated European efficiency of 98.7% for the SUN2000-60KTL-M0 [22]; grid-side parameters (PF = 1.000, f = 50.06 Hz) indicate a balanced operating snapshot. Reasoning:

because no plane-of-array irradiance record temporally overlaps the June 2026 PV log, Performance Ratio cannot be computed from this dataset without introducing an external assumption [4,5]. Conclusion: PR is reported as NOT_EVALUATED, and CF, efficiency, string availability, and DC power consistency are retained as the primary measured steady-state indicators.

Table 2. Steady-state key performance indicators.

KPI	Value	Benchmark	Status
Performance Ratio (PR)	NOT_EVALUATED	n/a—no overlapping POA irradiance	DATA GAP
Capacity Factor (CF)	15.48%	n/a—site-specific observed daily-equivalent CF	MEASURED
Inverter efficiency (η_inv)	98.72%	Huawei European efficiency 98.7% [22]	CONSISTENT
String availability (snapshot)	75.0%	100%	DEGRADED
MTD energy (June 2026)	5,429 kWh	n/a (no PR-based theoretical max)	MEASURED
DC power (live, snapshot)	25.49 kW	25.36 kW (inverter-reported)	CONSISTENT (0.5% diff.)

4.3. Snapshot power-loss quantification (persistent-condition scenario estimate)

Point: the three non-producing strings account for a measured, snapshot-instant DC shortfall of approximately 6,000 W, or 23.6% of the array's currently achievable capacity at this measurement. Evidence: **Table 3** quantifies this shortfall per string. Reasoning: extrapolating this single 08:16 WIB snapshot into a yearly energy or revenue figure requires assuming that the observed string-outage pattern persists, unchanged, for a full year an assumption this one-month dataset cannot validate, since string outages can be intermittent, seasonal irradiance differs from June conditions, and no repeated measurement confirms persistence. To avoid the term "annualized," which implies a validated forecast, this study labels the extrapolated figure a Persistent-Condition Scenario Estimate throughout. Conclusion: **Table 3** reports the measured snapshot shortfall as the primary, validated finding, and presents the scenario figure only as an explicit upper-bound planning heuristic IF the snapshot condition were to persist unchanged for a full year not a forecast, pending confirmation from continuous multi-month monitoring (Section 6, Limitations).

Table 3. Snapshot power-loss quantification and persistent-condition scenario estimate.

Component	Measured snapshot loss	Share of snapshot loss	Persistent-condition scenario estimate (hypothetical, not validated)
PV7 & PV8 (2 strings)	≈ 4,000 W	66.7%	≈ 12,000 kWh/yr (≈ Rp 18,000,000/yr)
PV6 (1 string)	≈ 2,000 W	33.3%	≈ 6,000 kWh/yr (≈ Rp 9,000,000/yr)
TOTAL	≈ 6,000 W	100%	≈ 18,000 kWh/yr (≈ Rp 27,000,000/yr) SCENARIO ONLY

Note: the inverter-thermal loss component and specific root-cause hypotheses (e.g., bypass-diode activation, cooling-system degradation) reported in the original submission are removed from this revision, as no on-site inverter- or ambient-temperature measurement exists in the acquired dataset to support them (Section 3.1); reintroducing them would repeat the definitive-diagnosis-from-a-single-snapshot pattern this methodology is designed to avoid.

4.4. Dynamic model: Measured temporal variability and historical weather results

Point: contrary to a reading of the dynamic model as "almost entirely NOT_EVALUATED," two of its three phenomenon classes day-to-day energy temporal variability and historical environmental variability are genuinely evaluated from measured data at their own appropriate (daily/hourly) resolution; only the sub-minute electrical-transient class remains unevaluated (Section 4.5). Evidence: of the 26 daily energy records available for June 2026, 23 qualified as valid full-day records (2 No-Data days and 1 partial day were excluded from ramp computation, not interpolated), yielding 21 valid day-to-day transitions (**Table 4**); the mean absolute daily ramp was 12.656%, with a median of only 2.823%, while the extrema reached +51.408% and −61.009%, and the daily energy standard deviation and coefficient of variation were 45.696 kWh and 19.449% respectively. Separately, the 2020–2025 historical hourly weather archive (irradiance and temperature) was fully evaluated at its native hourly resolution, though it does not temporally overlap the June 2026 PV output and is therefore not merged with it. Reasoning: the wide gap between the mean (12.656%) and median (2.823%) absolute ramp, together with the extreme values, indicates that day-to-day energy variability at this site is dominated by a small number of large-magnitude events rather than a uniform spread consistent with the No-Data/partial-day interruptions in the underlying log rather than with gradual weather-driven decline [23, 24]. Conclusion: this measured temporal and environmental variability is real, evaluated evidence in its own right, and is reported here as a distinct, evaluated layer of the dynamic model, separate from and not to be confused with the sub-minute electrical-transient characteristics addressed in Section 4.5, which remain not evaluable at this site's current instrumentation.

Table 4. Dynamic model: Measured temporal variability and historical weather summary.

Metric	Value	Status
Valid full-day records (of 26 available)	23 of 26	EVALUATED
Valid day-to-day transitions	21	EVALUATED
Mean |daily ramp|	12.656%	EVALUATED
Median |daily ramp|	2.823%	EVALUATED
Max positive daily ramp	+51.408%	EVALUATED
Max negative daily ramp	−61.009%	EVALUATED
Daily energy standard deviation	45.696 kWh	EVALUATED
Daily energy coefficient of variation (CV)	19.449%	EVALUATED
Historical hourly irradiance variability (2020–2025)	Evaluated historically; not paired with June 2026	EVALUATED
Historical hourly temperature variability (2020–2025)	Evaluated historically; not paired with June 2026	EVALUATED

4.5. Dynamic model: Electrical transient data requirements assessment

Point: unlike the temporal and environmental variability in Section 4.4, the prerequisites for sub-minute electrical dynamic characterization are absent at this installation (**Table 5**). Evidence: the available monitoring records do not contain synchronized sub-minute Pdc, Pac, Vdc, Idc, Vac, Iac, frequency, or irradiance time-series required to identify electrical rates of change and inverter transient response. Reasoning: dynamic MPPT and inverter studies use time-varying irradiance and time-resolved electrical measurements or experiments to quantify tracking and response behavior [13, 16]. Consequently, any response time, settling time, rate-of-change, or transient-loss value introduced here from an assumed time constant would describe a hypothetical simulation rather than the measured system [25]. Conclusion: electrical-transient characterization is therefore reported as NOT EVALUATED; this is a resolution- and instrumentation-driven limitation, not a negative finding about the Huawei inverter itself.

Table 5. Dynamic model electrical transient data requirements assessment.

Requirement	Actual status	Impact on dynamic model
High-frequency data (≤1 s)	Only hourly/daily aggregates	Cannot analyze transient events
MPPT V–I curve scanning	Single operating point only	Cannot optimize MPPT tracking
Real-time irradiance (pyranometer)	No on-site irradiance sensor	PR and transient loss cannot be evaluated
Weather transient data	No overlapping high-resolution record	Cannot detect cloud ramp events
Grid event log (ms resolution)	Single stable snapshot	No dynamic grid events detectable

4.6. Steady-state versus dynamic: Full parameter registry comparison

Responding directly to the request for a parameter-by-parameter comparison, and to ensure the Model Observability Score in Section 4.7 is traceable rather than arbitrary, **Table 6** reproduces the complete, a priori parameter registry (Section 3.4) underlying both models, with every row's applicability to each model declared independently of its outcome. Point: the two models are evaluable over largely non-overlapping parameter sets, and critically the dynamic model is not uniformly NOT_EVALUATED. Evidence: of the 16 parameters applicable to the dynamic model, 4 are EVALUATED (daily energy variability, daily energy CV, historical irradiance variability, historical temperature variability all detailed in **Table 4**), while the remaining 12 (string-level and electrical-domain parameters) are NOT_EVALUATED for lack of a synchronized time-series; of the 8 parameters applicable to the steady-state model, 7 are EVALUATED and only Performance Ratio is not. Reasoning: this pattern shows the two models to be complementary diagnostic layers addressing different physical time-scales instantaneous operating point versus day-to-day and historical variability versus sub-minute electrical transients rather than competing estimates of the same quantity. Conclusion: any future comparison should track parameter-level observability (**Table 6**) rather than a single combined score, consistent with the MOS/DRAI construction in Section 3.4; **Table 6** is also the exact source table from which the MOS values in Section 4.7 are counted, so the 7/8 and 4/16 denominators can be verified row by row rather than taken on faith.

Table 6. Steady-state versus dynamic: Full a priori parameter registry.

Parameter	Domain	SS Status	SS Result	Dynamic status	Dynamic result
PV string voltage	DC array	EVALUATED	Snapshot string voltages (**Table 1**)	NOT EVALUATED	No string-voltage time-series
PV string current	DC array	EVALUATED	Snapshot string currents (**Table 1**)	NOT EVALUATED	No string-current time-series
DC input power	Inverter	EVALUATED	25.361 kW	NOT EVALUATED	No electrical time-series
AC active power	Inverter	EVALUATED	25.036 kW	NOT EVALUATED	No electrical time-series
Inverter conversion efficiency	Inverter	EVALUATED	98.719%	NOT APPLICABLE	—
Snapshot string availability	DC array	EVALUATED	75.000%	NOT APPLICABLE	—
Observed daily equivalent CF	Energy	EVALUATED	15.480%	NOT APPLICABLE	—
Performance Ratio	Energy	NOT EVALUATED	No overlapping POA irradiance	NOT APPLICABLE	—
Daily energy variability	Temporal variability	NOT APPLICABLE	—	EVALUATED	Mean |ramp| = 12.656%
Daily energy CV	Temporal variability	NOT APPLICABLE	—	EVALUATED	19.449%

Table 6. *Cont.*

Parameter	Domain	SS Status	SS Result	Dynamic status	Dynamic result
Historical irradiance variability	Environmental variability	NOT APPLICABLE	—	EVALUATED	Hourly, 2020–2025 (not paired with June 2026)
Historical temperature variability	Environmental variability	NOT APPLICABLE	—	EVALUATED	Hourly, 2020–2025 (not paired with June 2026)
Electrical dPdc/dt	Electrical dynamics	NOT APPLICABLE	—	NOT EVALUATED	No electrical time-series
Electrical dPac/dt	Electrical dynamics	NOT APPLICABLE	—	NOT EVALUATED	No electrical time-series
Electrical dVac/dt	Electrical dynamics	NOT APPLICABLE	—	NOT EVALUATED	No electrical time-series
Electrical dIac/dt	Electrical dynamics	NOT APPLICABLE	—	NOT EVALUATED	No electrical time-series
Electrical df/dt	Grid dynamics	NOT APPLICABLE	—	NOT EVALUATED	No electrical time-series
Inverter response time	Electrical dynamics	NOT APPLICABLE	—	NOT EVALUATED	Requires identified transient event
Settling time/τ	Electrical dynamics	NOT APPLICABLE	—	NOT EVALUATED	No assumed time constant; measured transient required
Grid transient/RoCoF	Grid dynamics	NOT APPLICABLE	—	NOT EVALUATED	Requires sub-cycle frequency time-series

4.7. Model observability score and data resolution adequacy index

Point: read from the audited registry in **Table 6**, the steady-state model is observable for 87.5% of its applicable parameters (7 of 8), versus 25.0% for the dynamic model (4 of 16). Evidence: **Table 7** shows that the steady-state model evaluates every applicable parameter except Performance Ratio, whereas the dynamic model evaluates its daily temporal-variability and historical-weather parameters but none of its electrical- or grid-dynamics parameters. **Table 8** distinguishes native dataset time scales from reference-backed electrical-dynamic requirements. Daily energy and hourly weather are evaluated at their actual native intervals. For power-ramp analysis, a five-minute criterion is used as a conservative study threshold consistent with utility-scale PV ramp analyses employing minute-scale data [26]. For inverter transient identification, a one-second study criterion is adopted to ensure several samples across second-scale dynamic behavior and is consistent with dynamic MPPT and measured inverter-response studies [10, 11]. For grid frequency/RoCoF observability, the 0.02 s criterion corresponds to a 50-frame/s reporting interval available for 50-Hz synchrophasor systems under IEEE/IEC 60255-118-1 [9]. Where no electrical timestamp exists, DRAI is left undefined rather than assigned zero. Reasoning: the 87.5%-versus-25.0% gap therefore quantifies the present instrumentation boundary, not model superiority. Conclusion: MOS and DRAI are reported as separate, auditable diagnostics and are not combined into an arbitrary overall ranking.

Table 7. Model Observability Score (MOS), audited against the a priori registry (**Table 6**).

Model	Applicable parameters	Evaluated parameters	MOS (%)
Steady-State	8	7	87.5
Dynamic—all applicable parameters	16	4	25.0
of which: temporal/environmental sub-domain	4	4	100.0
of which: electrical/grid-dynamics sub-domain	12	0	0.0

Table 8. Data Resolution Adequacy Index (DRAI), with declared reference basis.

Phenomenon	Δt required (ref.)	Δt actual	Status	Reference basis
Energy variability (day-to-day)	86,400 s	86,400 s	ADEQUATE	Native daily record; monitoring framework [4]
Environmental variability	3,600 s	3,600 s	ADEQUATE	Native hourly weather archive (study dataset)
Power ramp-rate analysis	300 s	undefined—no timestamp	NOT_EVALUATED	Minute-scale PV ramp analysis [26]
Inverter response time	1 s	undefined—no timestamp	NOT_EVALUATED	Dynamic MPPT/inverter-response studies [10, 11]
Grid transient/RoCoF	0.02 s	undefined—no timestamp	NOT_EVALUATED	IEEE/IEC synchrophasor reporting framework [9]

4.8. Interannual energy production variability

Point: annual production for 2022–2026 (2026 partial) shows substantial year-to-year variation without a monotonic trend (**Figure 1**): approximately 58, 92, 52, 75, and 41 MWh, respectively. Evidence: 2023 was the highest year and 2024 the lowest full year, a −43% change year-on-year. Reasoning: annual energy is jointly influenced by weather, operational availability, maintenance, outages, and the completeness of the observation period. Published degradation reviews show that long-term degradation estimation requires qualified time-series data and appropriate statistical methodology; field degradation rates are generally much smaller than the year-to-year swings visible here [10, 11]. Conclusion: no degradation trend or single root cause is asserted from this figure. A multi-year, irradiance-normalized analysis with overlapping irradiance measurements is required before any degradation-rate claim can be supported.

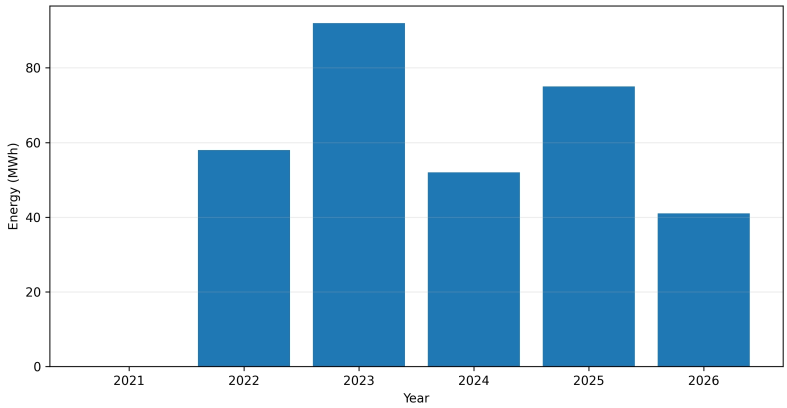

Figure 1. Annual energy production, 2022–2026 (2026 partial year); reported descriptively, not as a confirmed degradation trend.

4.9. String-level monitoring visualization

Figure 2 presents the measured string-level voltage, current, and calculated power (V × I) from the 26 June 2026 snapshot, visually distinguishing the nine producing strings from PV6 (zero-current/high-voltage) and PV7–PV8 (zero-current/low-voltage). This revision replaces the original six-panel dashboard, whose Panel 6 (synthetic cloud-passing simulation) and Panel 7 KPI card (fabricated inverter-temperature and assumed-PSH Performance Ratio entries) are removed in this version, consistent with Sections 3–4; the corresponding source dashboard script should be regenerated by the authors to drop those two panels before resubmission.

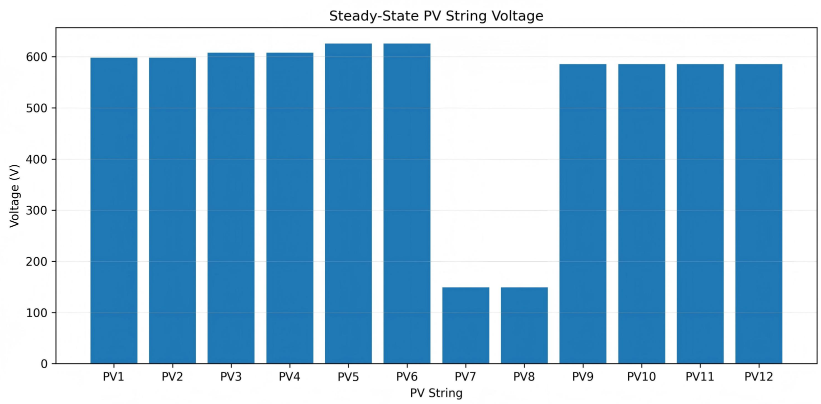

Figure 2. *Cont.*

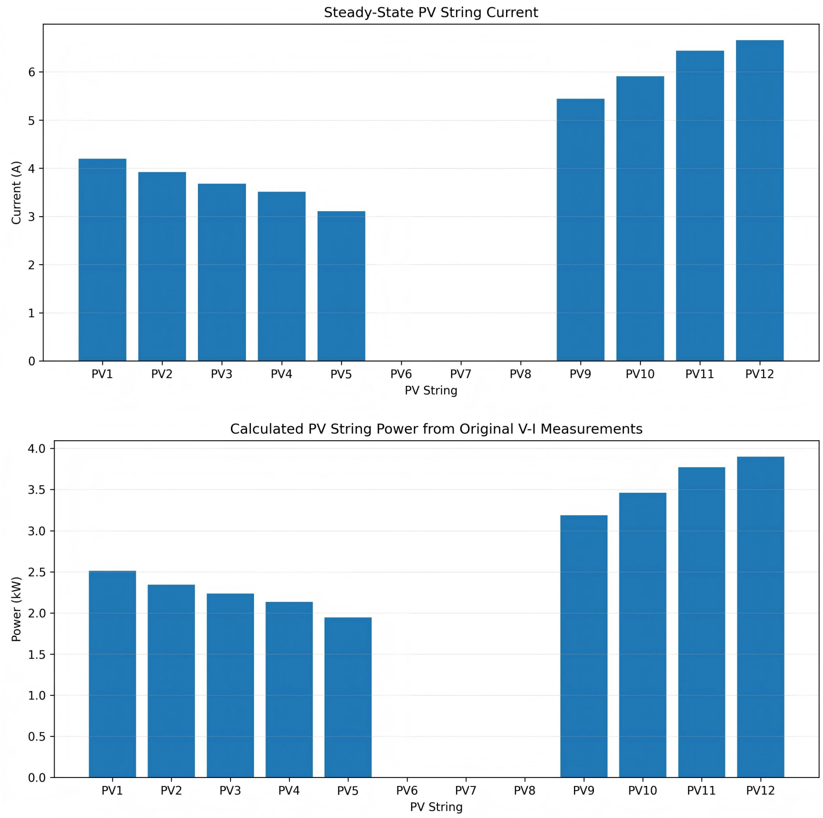

Figure 2. Measured PV string voltage, current, and calculated power, 26 June 2026 snapshot.

5. Instrumentation roadmap and observability-driven recommendations

Based on the MOS and DRAI results (Section 4.7), the steady-state model is the appropriate framework for immediate deployment at this installation, while the dynamic model's temporal- and environmental-variability sub-domain is also usable with the present records. Rather than allocating an arbitrary percentage between the two paradigms, the proposed roadmap links each instrumentation phase to a specific observability gap. Phase 1 (immediate, no new hardware): formalize steady-state string monitoring, DC/AC consistency checks, and daily energy variability reporting. Phase 2 (3–6 months): install a calibrated plane-of-array irradiance sensor and temperature sensing consistent with accepted PV monitoring practice [4]; this resolves the present PR data gap and provides a basis for irradiance-normalized performance analysis. Phase 3 (6–12 months): deploy synchronized electrical logging at a sampling rate appropriate to the targeted transient phenomena. Dynamic MPPT test literature and measured inverter-dynamics studies demonstrate the need for time-resolved electrical data for this purpose [13,14]. If grid RoCoF or synchrophasor-class behavior is a target, the acquisition architecture should also be selected with the relevant synchronized phasor-measurement requirements in mind [9]. Only after these data are available should a site-specific dynamic model be fitted to measured transients rather than an assumed time constant.

6. Conclusion

This study revisited the JST PV Farm case study under an observability-first principle: every reported KPI is either computed directly from measured data or explicitly flagged as NOT_EVALUATED against an a priori parameter registry, with no assumed peak-sun-hour value, inverter time constant, or fabricated sensor reading used to fill a data gap. Three principal conclusions are drawn. First, string-level steady-state screening identified two distinct measured-condition anomalies PV6 (zero-current/high-voltage) and PV7/PV8 (zero-current/low-voltage) accounting for a measured snapshot DC shortfall of approximately 6.0 kW (23.6% of currently achievable capacity); a Persistent-Condition Scenario Estimate of this shortfall (≈18,000 kWh/yr, ≈Rp 27,000,000/yr) is reported strictly as a planning heuristic, explicitly not a validated forecast, pending confirmation from continuous multi-month monitoring. Second, the dynamic model is genuinely and demonstrably evaluated for day-to-day energy temporal variability (mean absolute daily ramp 12.656%, CV 19.449%) and historical hourly weather variability (2020–2025); only its sub-minute electrical-transient sub-domain inverter response time, ramp-rate behavior, and transient loss during cloud-passing events remains NOT_EVALUATED, a direct, quantified consequence of the absence of sub-minute electrical logging at this site, not a finding about inverter dynamics themselves and not a verdict on the dynamic paradigm as a whole. Third, an audited Model Observability Score (87.5% steady-state, 7 of 8 parameters, vs. 25.0% dynamic overall but 100% for its temporal/environmental sub-domain and 0% for its electrical sub-domain, 4 of 16 parameters) and a reference-backed Data Resolution Adequacy Index together quantify this gap transparently and traceably, and point to a specific, phased instrumentation investment (Section 5) capable of closing it, without resorting to an arbitrary combined weighting between the two modeling paradigms.

Limitations: this analysis is based on a single measurement snapshot (26 June 2026) and one month of daily aggregates (June 2026); the string-availability pattern, string-level anomalies, and interannual-energy variation discussed above should not be assumed to persist unchanged across seasons or years without repeated measurement. No irradiance-normalized, multi-year degradation analysis is possible until the Phase-2 pyranometer installation (Section 5) provides an overlapping irradiance record; consequently, no degradation rate is estimated or implied by the 2022–2026 interannual energy pattern in Section 4.8. All root-cause language in this revision is confined to measured-condition labels rather than confirmed diagnoses, consistent with the evidentiary limits of a single V–I snapshot. The MOS and DRAI registries (**Tables 6–8**) are declared a priori in the accompanying analysis code and are provided as supplementary CSV output for independent audit; the verified reference basis for each DRAI row is stated directly in **Table 8** and retained in the final bibliography.

Future work should prioritize the Phase-2 and Phase-3 instrumentation described in Section 5, followed by (i) a full irradiance-normalized Performance Ratio and degradation-trend analysis once overlapping irradiance data are available, and (ii) genuine dynamic-model fitting from measured sub-minute electrical time-series, rather than an assumed inverter time constant.

Author contributions: Conceptualization, DP and RA; methodology, software, formal analysis, investigation, data curation, visualization, and original draft preparation, DP; validation, review, and editing, RA, MK, and NAO; supervision, RA, MK, and NAO. All authors have read and approved the final manuscript.

Funding: This work received no external funding.

Institutional review board statement: This study did not involve human participants, animals, or personal data; therefore, institutional review board approval was not required.

Informed consent statement: Informed consent was not applicable because this study did not involve human participants.

Data availability statement: The data used in this study are available from the corresponding author upon reasonable request.

Acknowledgment: The authors sincerely thank Universitas Negeri Yogyakarta, Universitas Islam Nahdlatul Ulama Jepara, and the Doctoral Program in Engineering Science for their academic support.

Conflict of interest: The authors declare no conflict of interest.

AI use statement: During the preparation of this manuscript, the authors used ChatGPT solely for language refinement. No AI tools were used for data analysis, interpretation, or generation of scientific content. All outputs were critically reviewed and edited by the authors. The authors take full responsibility for the integrity and accuracy of the work.

References

1. Madeti SR, Singh SN. Monitoring system for photovoltaic plants: A review. Renewable and Sustainable Energy Reviews. 2017; 67: 1180–1207. doi: 10.1016/j.rser.2016.09.088
2. Prihatmoko D, Asnawi R, Khairudin M. Optimizing the Utilization of 1.35 MW Grid-Connected Solar Power Plants to Reduce Carbon Emissions in the PLN Electricity System. IOP Conference Series: Earth and Environmental Science. 2025; 1543(1): 012032. doi: 10.1088/1755-1315/1543/1/012032
3. Huld T, Müller R, Gambardella A. A new solar radiation database for estimating PV performance in Europe and Africa. Solar Energy. 2012; 86(6): 1803–1815. doi: 10.1016/j.solener.2012.03.006
4. IEC. IEC 61724-1:2021, Photovoltaic System Performance—Part 1: Monitoring, 2nd ed. International Electrotechnical Commission; 2021. Available online: https://webstore.iec.ch/en/publication/65561
5. Reich NH, Mueller B, Armbruster A, et al. Performance ratio revisited: Is PR > 90% realistic? Progress in Photovoltaics: Research and Applications. 2012; 20(6): 717–726. doi: 10.1002/pip.1219
6. Li X, Wen H, Hu Y, et al. A Comparative Study on Photovoltaic MPPT Algorithms under EN50530 Dynamic Test Procedure. IEEE Transactions on Power Electronics. 2021; 36(4): 4153–4168. doi: 10.1109/TPEL.2020.3024211
7. Poudel B, Guruwacharya N, Subedi S, et al. Experimentation in Exploring Photovoltaic Inverter Dynamics under Different Irradiance Levels through a Data-Driven Approach. IEEE Access. 2024; 12: 164137–164150. doi: 10.1109/ACCESS.2024.3488493
8. IEEE/IEC 60255-118-1:2018. Measuring Relays and Protection Equipment—Part 118-1: Synchrophasor for Power Systems—Measurements. IEEE/IEC; 2018. Available online: https://standards.ieee.org/ieee/60255-118-1/5724/
9. Villalva MG, Gazoli JR, Filho ER. Comprehensive Approach to Modeling and Simulation of Photovoltaic Arrays.

IEEE Transactions on Power Electronics. 2009; 24(5): 1198–1208. doi: 10.1109/TPEL.2009.2013862
10. Phinikarides A, Kindyni N, Makrides G, et al. Review of photovoltaic degradation rate methodologies. Renewable and Sustainable Energy Reviews. 2014; 40: 143–152. doi: 10.1016/j.rser.2014.07.155
11. Jordan DC, Kurtz SR. Photovoltaic Degradation Rates—An Analytical Review. Progress in Photovoltaics: Research and Applications. 2013; 21(1): 12–29. doi: 10.1002/pip.1182
12. Guerriero P, Piegari L, Rizzo R, et al. Mismatch Based Diagnosis of PV Fields Relying on Monitored String Currents. International Journal of Photoenergy. 2017; 2017: 2834685. doi: 10.1155/2017/2834685
13. Dhimish M, Holmes V. Fault detection algorithm for grid-connected photovoltaic plants. Solar Energy. 2016; 137: 236–245. doi: 10.1016/j.solener.2016.08.021
14. Madeti SR, Singh SN. A comprehensive study on different types of faults and detection techniques for solar photovoltaic system. Solar Energy. 2017; 158: 161–185. doi: 10.1016/j.solener.2017.08.069
15. Ahmed J, Salam Z. A Modified P&O Maximum Power Point Tracking Method with Reduced Steady State Oscillation and Improved Tracking Efficiency. IEEE Transactions on Sustainable Energy. 2016; 7(4): 1506–1515. doi: 10.1109/TSTE.2016.2568043
16. Belkaid A, Colak I, Isik O. Photovoltaic maximum power point tracking under fast varying of solar radiation. Applied Energy. 2016; 179: 523–530. doi: 10.1016/j.apenergy.2016.07.034
17. Lappalainen K, Valkealahti S. Recognition and modelling of irradiance transitions caused by moving clouds. Solar Energy. 2015; 112: 55–67. doi: 10.1016/j.solener.2014.11.018
18. Skomedal ÅF, Øgaard MB, Haug H, et al. Robust and Fast Detection of Small Power Losses in Large-Scale PV Systems. IEEE Journal of Photovoltaics. 2021; 11(3): 819–828. doi: 10.1109/JPHOTOV.2021.3060732
19. Meng B, Loonen RCGM, Hensen JLM. Leveraging dynamic power benchmarks and CUSUM charts for enhanced fault detection in distributed PV systems. Energy Conversion and Management. 2024; 314: 118692. doi: 10.1016/j.enconman.2024.118692
20. Dhimish M, Tyrrell AM. Photovoltaic bypass diode fault detection using artificial neural networks. IEEE Transactions on Instrumentation and Measurement. 2023; 72: 1–10.
21. Zhao Y, de Palma JF, Mosesian J, et al. Line–line fault analysis and protection challenges in solar photovoltaic arrays. IEEE Transactions on Industrial Electronics. 2013; 60(9): 3784–3795. doi: 10.1109/TIE.2012.2205355
22. Huawei Technologies Co., Ltd. SUN2000-60KTL-M0 Smart String Inverter—Technical Specifications. Available online: https://solar.huawei.com/-/media/Solar/attachment/pdf/au/datasheet/SUN2000-60KTL-M0.pdf (accessed on 13 July 2026).
23. Mellit A, Kalogirou S. Assessment of machine learning and ensemble methods for fault diagnosis of photovoltaic systems. Renewable Energy. 2022; 184: 1074–1090. doi: 10.1016/j.renene.2021.11.125
24. Lappalainen K, Valkealahti S. Output power variation of different PV array configurations during irradiance transitions caused by moving clouds. Applied Energy. 2017; 190: 902–910. doi: 10.1016/j.apenergy.2017.01.013
25. Agüera-Pérez A, Espinosa-Gavira MJ, Palomares-Salas JC, et al. Meteorological contexts in the analysis of cloud-induced photovoltaic transients: A review. Renewable and Sustainable Energy Reviews. 2024; 202: 114689. doi: 10.1016/j.rser.2024.114689
26. Mazumdar BM, Saquib M, Das AK. An empirical model for ramp analysis of utility-scale solar PV power. Solar Energy. 2014; 107: 44–49. doi: 10.1016/j.solener.2014.05.027